Molecular Dynamics Study of the Beryllium Interaction with C-S-H Phases

Iuliia Androniuk,* Nese Çevirim-Papaioannou, Marcus Altmaier, and Xavier Gaona

ABSTRACT: Beryllium has applications in fission and fusion reactors, and accordingly it is expected in specific w aste s treams i n n uclear waste repositories. As a part of the multi-barrier system, cementitious materials were shown to strongly sorb beryllium, but the precise uptake mechanisms remain ill-defined. C omputational s imulations w ere u sed t o s tudy Be(II) uptake by calcium-silicate-hydrate (C-S-H) phases. Molecular dynamics (MD) calculations show that Be(II) sorbs on (001), (004), and (100) C-S-H surfaces through Ca-bridges and hydrogen bonds. Energy profiles indicate that surface complexes with the highest number of Ca-bridges are the most stable. MD simulations support also Be(II) retention in the C-S-H interlayer. $Be(OH)_3^-$ is predominantly bound through the exchange of water molecules for deprotonated silanol groups or through multiple Ca-bridges, whereas $Be(OH)_4^{2-}$ is immobilized in the interlayer midplane. These results provide key inputs to understand the mechanisms driving Be(II) uptake by cementitious materials of relevance in the context of nuclear waste disposal.

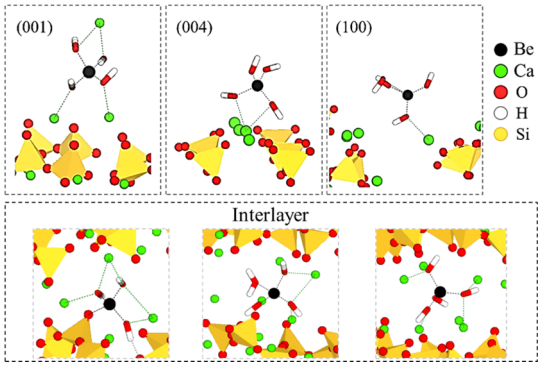

1. INTRODUCTION

Beryllium is a lightweight metal with unique physical and chemical properties that can be used as a neutron reflector, neutron moderator, and neutron multiplier in research fission reactors. The operating life of these materials is limited due to the gradual build-up of helium and tritium.[1,2] Accordingly, beryllium is found in certain waste streams disposed of in repositories for nuclear waste. Due to its high toxicity, it is important to understand retention mechanisms and investigate the molecular mechanisms of its interaction with all components of the waste disposal system.

Cementitious materials are often used in the design and construction of radioactive waste repositories, and thus are a relevant part of the multibarrier system (e.g., as principal construction material, part of packaging for certain types of waste, sealing material for storage cells) . Calcium-silicate-hydrate (C-S-H) is the main binding phase of cement and one of the components that defines i ts s orption properties.[3,4] Molecular dynamics simulations have been successfully used to model cementitious materials. The C-S-H phases have a complex nanocrystalline structure that is challenging to precisely model on the molecular level. Therefore, big simulation cells and long simulation times are usually required. Modeling is typically done using tobermorite as the closest mineral structure[5−9] and can involve different s urfaces, i.e., (001), (004), and (100). The structural organization of the C-S-H interlayer is not well understood and only a few studies have been done to describe it. The behavior of confined water in the C-S-H interlayer was studied by Youssef et al.[10] using molecular dynamics simulations. In their work, the interlayer was modeled as quasi-two-dimensional nanopores with a width less than 1 nm. It was found that the disordered structure of C-S-H provides multiple acceptor sites for hydrogen bonds, and therefore is significantly more hydrophilic compared to cationic clays that are often used for comparison. Abdolhosseini Qomi and co-workers[8] constructed bulk C-S-H models that correspond to a wide range of compositions that could be used successfully to study both the mechanical and the sorption properties of C-S-H.[11,12]

A number of computational studies describe the behavior of beryllium in aqueous solutions on the molecular level. Beryllium preferentially coordinates ligands in tetrahedral geometry, has strong hydrolyzing and polarizing abilities, and shows complex pH-dependent solution chemistry.[13−15] In alkaline and highly alkaline conditions, typical for cementitious environments, it exists in the form of $Be(OH)_3^-$ and $Be(OH)_4^{2-}$ hydrolysis species.[16] In previous sorption studies, the uptake of beryllium by cementitious materials could not be explained exclusively as a surface complexation process, and the incorporation into the C-S-H interlayer was suggested as

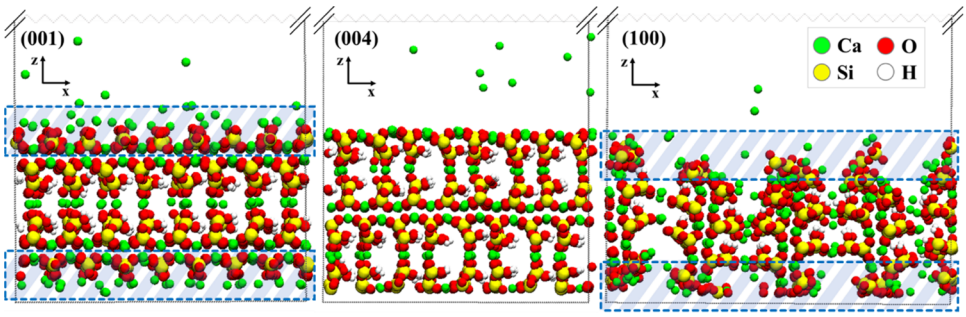

Figure 1. Models of (001), (004), and (100) surfaces of C-S-H considered in this work. Water molecules and aqueous hydroxyls have been omitted for clarity. The marked blue zones show the modified layers. For the (004) surface initial tobermorite structure was used.

one of the possible uptake mechanisms.[17] Our first attempts to model the C-S-H/Be(II) system were limited to the surface processes and focused on the surface (001). The main conclusions were that the $Be(OH)_3^-$ and $Be(OH)_4^{2-}$ species are sorbed to the (001) surface OH-groups through Ca-bridges, and three preferable surface complexes were identified: $>Ca_2Be(OH)_3$ (Ca bound to 3 deprotonated silanol groups), $>CaBe(OH)_3$ (Ca bound to 2 deprotonated silanol groups), and $>Ca_3Be(OH)_4$ (Ca coordinated with 3 deprotonated silanol groups).

This study further extends our experimental and modeling efforts on the retention of beryllium by cementitious materials.[16−18] For this purpose, we used a combination of classical and constrained molecular dynamics simulations to gain insight into the molecular mechanisms involved in the uptake of beryllium by C-S-H phases with a high Ca/Si ratio, including both surface processes and incorporation on the C-S-H interlayer. With time, C-S-H phases can degrade through decalcification and dissolution phenomena, involving also changes on the surface properties and solution composition, i.e., sorption sites, pH, Ca concentration, etc. These processes are important because they will also affect the Be uptake mechanisms. Unfortunately, it is not possible to observe this phenomenon with classical molecular dynamics, and therefore degradation processes are out of the scope of this study. The surfaces for the molecular dynamics study were chosen according to their abundance and stability in tobermorite: (001), (004), and (100). The (001) surface is a natural cleavage plane for the tobermorite group of minerals.[19] It is also expected that stable surfaces are those in which silicate bonds are broken on cleavage. The recent theoretical study using the first-principles simulations has shown that the (004) surface is the most stable followed by the (100) surface (with a surface energy of 0.41 and 0.54 J/m^2 respectively).[20] Therefore, the (004) surface has been chosen to represent an additional basal surface (the tobermorite structure was used for this surface in this study), and the (100) surface − the edge surface of the C-S-H particle in this study. The model of the interlayer presented in our work was developed based on a recent study on the hydration properties and structural organization of synthetic C-S-H by Gaboreau et al.,[21] and it is built similarly to the interlayer model (the "Model A") reported by Svenum et al.[22]

2. COMPUTATIONAL DETAILS

The models for (001), (004), and (100) surfaces were built based on the models proposed by Jamil and co-authors.[23] The Ca/Si ratio was not represented precisely by the number of Ca and Si atoms in the systems, but rather by introducing the main features of the interface: structural defects, deprotonation, and ion speciation in the interface (Figure 1).

To maintain the overall stability of the models without freezing the surface during simulations, only the silicate layers of (001) and (100) surfaces in contact with the solution have been modified (the areas marked blue in Figure 1). Several experimental studies have found that for C-S-H phases with a high Ca/Si ratio (∼1.6) the mean chain length in the silicate layer is around 2.3.[24,25] Thus, the bridging Si were removed to obtain the structure of C-S-H with Ca/Si > 1.4, so the surface silicate layer is composed only of dimers of pairing Si. In real C-S-H phases, bridging Si is still present in the structure (12−25% of total Si),[21] but layer stacking variations and fragments of portlandite are also possible, which influence the total Ca/Si ratio. We decided to remove all of the bridging Si as a compromise to reach a higher Ca/Si ratio without adding too many Ca^{2+} cations to the model. The silanol groups of the pairing Si were deprotonated according to theoretical considerations for the surface of C-S-H with high pH values.[26] The missing bridging Si atoms were replaced by Ca^{2+} and $CaOH^+$ to neutralize the negative charge. The C-S-H layers in the middle of the surface were not modified. The (004) surface was unstable after modification; therefore, we chose to maintain the initial structure of tobermorite to study the interaction of beryllium hydroxide species with the structural calcium layer. The interfacial aqueous solution contained 6 ions of $Be(OH)_3^-$, and 4$Be(OH)_4^{2-}$ with ∼5400 H_2O molecules, roughly corresponding to a concentration of beryllium ions of 0.1 M and a pH of ∼12.7, as estimated using thermodynamic data reported in Çevirim-Papaioannou et al.[16] Atoms of Be^{2+} together with aqueous hydroxyls were randomly inserted into the solution layer at distance > 0.1 nm from the surface (the initial positions are listed in Table S3 in the Supporting Information), the introduced negative charge was neutralized by adding aqueous Ca^{2+} ions. The summary of the C-S-H surface simulation cells can be found in Table S1 in the Supporting Information.

The ClayFF interatomic interaction parameters have been used for C-S-H as they have been shown to be reliable and accurate for cement/water interface simulations.[27−31] Water was described using the extended simple point charge (SPC/E) model.[32] The 12-6-4 Lennard-Jones type non-bonded parameters for Ca^{2+} and Be^{2+} for SPC/E water, which include the contribution from the ion-induced dipole interaction, were taken from Li and Merz.[33,34] The surface deprotonated oxygen atoms were assigned a partial charge of $q_{onb} = -1.3|e|$, higher than the protonated ones in the standard ClayFF model.[9,35,36]

The parameters used in this work are shown in Table S2 in the Supporting Information.

Standard Lorenz−Berthelot mixing rules[37] were applied to calculate short-range Lennard-Jones interactions between the unlike atoms (with a cut-off distance of 1.4 nm). Long-range electrostatic forces were evaluated by means of the Ewald summation method. All molecular dynamics (MD) simulations were performed using the LAMMPS software package (March 3, 2020 version).[38] The equilibration of the model was carefully monitored by assessing the temperature, pressure, kinetic, and potential energy of the system, and dimensions of the simulation box, to confirm that these parameters reach their equilibrium steady-state values on average.[39]

All C-S-H models were equilibrated for 5 ns in the *NPT* ensemble prior to introducing Be species. The Newtonian equations of the atomic motions were numerically integrated with a timestep of 1 fs, and the model systems were initially equilibrated for 5 ns in the isobaric−isothermal statistical ensemble (*NPT*), then for 5 ns in the canonical ensemble (*NVT*). Temperature and pressure were constrained using the Nose−Hoover thermostat and barostat[37] under ambient conditions (T = 295 K, P = 0.1 MPa). To avoid drifting of the modeled systems, four Si atoms from each surface were immobilized during *NVT* production runs, but they were still allowed to interact with other atoms. The VMD software package (version 1.9.3) has been used for visualization.[40]

Recent advances in the experimental description of the C-S-H interlayer structure helped us to modify and adjust the existing approach to C-S-H interlayer modeling. The atomistic model was built from the initial structure of tobermorite 1.4 nm ($Ca_5Si_6O_{16}(OH)_2{\cdot}7H_2O$).[41] The crystallographic unit cell has been multiplied (6 × 6 × 2) to create a relatively large simulation supercell to accumulate better statistical data. All bridging silicon tetrahedra in the interlayer were removed and replaced by interlayer calcium ions, and all the non-bridging silanol groups were left deprotonated. The amount of interlayer water was adjusted to match the proportion of water-to-interlayer calcium provided for C-S-H with a high Ca/Si ratio in Gaboreau et al.:[21] $H_2O/Ca_{interlayer} \approx 2.5$. The high stability of the C-S-H model with low water content (H_2O/Si = 1.4 for Ca/Si = 1.6) was previously confirmed by a combination of molecular modeling and quantum chemistry calculations by Kovačević et al.[42] The final model has 4 interlayers and consists of 2304 Si, 2304 $Ca_{CaO\text{-}layer}$, 1152 $Ca_{interlayer}$, and 2909 O_{water} atoms. Some water molecules were transformed into aqueous hydroxyls (310 OHw) to match the expected proportion of divalent (Ca^{2+}) and monovalent ($CaOH^+$) cations reported in Gartner et al.:[43] $CaOH^+/Ca^{2+} \approx 0.25$ at pH = 12.7.

First, a simulation without beryllium was performed in the *NPT* (5 ns) and *NVT* (5 ns) ensembles to verify the stability of the interlayer model and to equilibrate it (Figure S1 in the Supporting Information). Cell dimensions after equilibration were 7.742 × 7.742 × 46.748 nm^3, with an interlayer distance of 1.1687 nm on average. This value is only slightly higher than the value of 1.12 nm, reported for C-S-H with Ca/Si > 1.5,[44] but less than the distance of 1.23 nm described for fully hydrated C-S-H phases with Ca/Si > 1.2 in Gaboreau et al.[21] Real C-S-H phases are not continuous in x and y directions, as modeled in our work, and there might be higher disorder, inclusion of portlandite fragments, stacking variations, etc., that can affect the interlayer distance. Then 12 beryllium hydroxo complexes were introduced in the middle of the interlayers (two $Be(OH)_3(OH_2)^-$ and one $Be(OH)_4^{2-}$ in each), the overlapping water molecules were moved to a different part of the interlayer. The cell was equilibrated once again in two steps, and finally the MD production run was performed in the *NVT*-ensemble for 20 ns with a timestep of 1 fs under ambient conditions. Total electroneutrality of the simulation cell was ensured by balancing the number of counterions in the interlayer. Cell dimensions after equilibration with the Be species were 7.741 × 7.741 × 46.740 nm^3, with an interlayer distance of 1.1685 nm on average. There was no detectable change in the interlayer space distance after the insertion of the Be atoms.

To describe local structural properties, running coordination numbers, and density profiles were calculated. The coordination numbers for selected pairs of atoms are estimated with the following formula

$$n(r') = 4\pi\rho \int_0^{r'} g(r) r^2 \, dr \tag{1}$$

where $g(r)$ is the radial distribution function, ρ is the bulk density, r is the distance between the atoms.

Atomic density profiles in the direction perpendicular to the surface are calculated by evaluating of the average number of atoms of a certain type ($\bar{N}_A$) found within the range of distances from z to $z + \Delta z$ parallel to the surface

$$\text{density}_A = \frac{\bar{N}_A(\Delta z)}{V} \tag{2}$$

where V is the total volume of the simulation cell. Δz = 0.01 nm. The shape, position, and number of peaks on the density profiles provide information on the preferential binding and mobility of atoms during the simulation (e.g., multiple peaks correspond to different binding probabilities; single intense peak shows a preferential geometry; wide peak of low intensity signifies higher mobility/diffusivity). The two-dimensional distribution in the xy plane was calculated to determine the preferential sorption sites for beryllium species. Distributions are defined by the probability of finding an atom of type A in a position (x, y) above the surface within a distance range from z to $(z + \Delta z)$

$$\text{surface density}_A(x, y) = \bar{N}_A(\Delta x \Delta y) \tag{3}$$

where Δz = 0.1−0.5 nm, $\Delta x = \Delta y$ = 0.02 nm.

The potential of mean force (PMF) calculations were applied to obtain a quantitative description of the adsorption free energy profiles of beryllium as a function of its distance from the C-S-H surfaces. The "umbrella sampling" algorithm[45] allows overcoming high-energy barriers and sampling unfavorable atomic configurations of the system with a statistical accuracy that would otherwise not be possible. This method is very precise but computationally expensive; therefore, only the most common sorption sites, shown by classical MD simulations, were selected for each surface studied. The COLVARS module implemented in the LAMMPS software package[46] was used to perform umbrella sampling calculations. The weighted histogram analysis method (WHAM)[47] was used to calculate the PMF curves from the umbrella sampling data. A complete calculation requires a number of separate simulations, and for each PMF curve obtained, approximately 120 biased MD simulations were run in the *NVT* ensemble for 2 ns time each to cover the complete reaction coordinate. The z-distance between the topmost atoms of the surface and

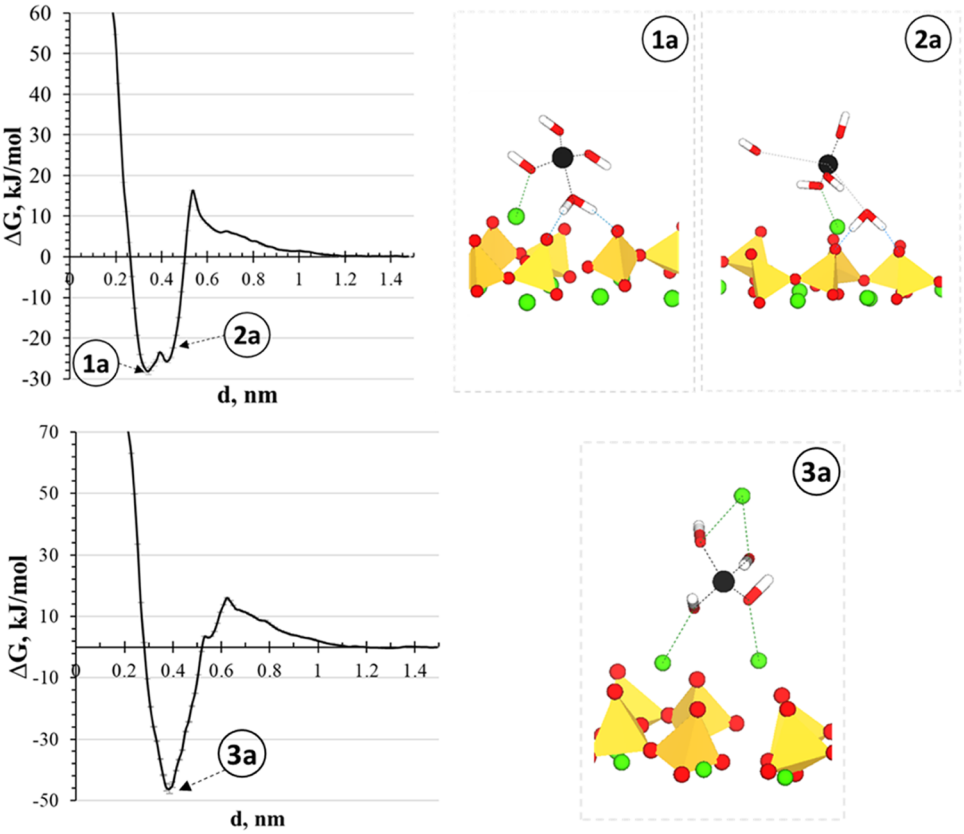

Figure 2. PMF curve for $Be(OH)_3(OH_2)^-$ (top) and $Be(OH)_4^{2-}$ (bottom) sorption on the (001) surface of C-S-H with snapshots of the defined surface complexes (see Figure S2 in the Supporting Information for the corresponding RCN plots; color scheme here and in the following depicted molecular surface structures as follows: Si – yellow; Ca – green; O – red; H – white; Be – black).

beryllium was chosen as a collective variable. All simulations at defined windows are independent and could be run in parallel. The Monte Carlo bootstrapping approach implemented in the WHAM algorithm has been used to assess statistical uncertainties.[47,48]

3. RESULTS AND DISCUSSION

3.1. Sorption on the (001) Surface. The typical sorption sites and surface complexes for beryllium on the (001) surface of C-S-H have been discussed in detail in our previous publications.[17,18] It was shown that the Ca^{2+} distribution on the (001) surface of C-S-H plays a key role in the adsorption mechanisms of beryllium. On the (001) surface of C-S-H, the bridging Si atoms were replaced by Ca^{2+} and additional Ca ions were added to the solution, with a total of 76 Ca atoms on the surface initially, and 66 Ca atoms after the equilibration. Few cations diffused in the solution, but the overall Ca^{2+} sorption layer remained stable, see density profile reported in previous work.[17] It is generally accepted that calcium ions are strongly attracted to negatively charged silanol groups and form a surface layer that changes the overall surface charge from negative to positive.[49,50] Of the 10 species of Be introduced at the interface, 8 were sorbed by the surface on average during the classical MD simulation run, suggesting favorable sorption on this surface. However, the energetical parameters of the complexation of Be(II) on the (001) surface of C-S-H have not yet been quantified. Therefore, here we additionally present the results of potential of mean force calculations (PMF) performed for $Be(OH)_3(OH_2)^-$ and $Be(OH)_4^{2-}$ species. The position of $d_{CSH\text{-}Be}$ = 0 nm is defined at the average position of the topmost surface oxygens. The *xy* position on top of the surface was not constrained, as our previous MD study revealed dominant nonspecific adsorption on the C-S-H surface: anionic species of beryllium are bound to surface calcium cations.

The free energy of adsorption of $Be(OH)_3(OH_2)^-$ on C-S-H surfaces is shown in Figure 2. On the PMF curve two minima ~0.1 nm apart from each other can be identified (surface complexes **1a** and **2a**). It represents a very stable surface complex with an energy barrier of around 40 kJ/mol. For the PMF minima found, the running coordination numbers (RCN) for pairs of atoms were additionally calculated to describe the complexes (Figure S2 in the Supporting Information).

The first minimum is found at $d_{CSH\text{-}Be} \approx 0.34$ nm ($\Delta G_{min} = -28.22 \pm 0.74$ kJ/mol), when beryllium bonds to the surface through the "OH-bridge" with the surface Ca, additionally stabilized by H-bonds formed between its water molecule and deprotonated silanol groups (the surface complex **1a**). The second minimum at $d_{CSH\text{-}Be} \approx 0.43$ nm ($\Delta G_{min} = -25.76 \pm 0.28$ kJ/mol; the surface complex **2a**) corresponds to the transition binding of $Be(OH)_3(OH_2)^-$ to the surface of C-S-H, in which beryllium shares a hydroxyl group with the surface calcium cation, the water molecule of the initial aqueous complex is exchanged for the water molecule bound to the surface through two H-bonds. The snapshot **2a** in Figure 2 has caught the exchange moment when the distance between Be and the two water molecules is greater than the equilibrium distance. This exchange partially contributes to the high energy barrier and the stronger binding energy. Consequently, only

0.5 water molecules are present in the first coordination sphere of Be (see the calculated RCN for the surface complex **2a** in Figure S3 in the Supporting Information).

The bottom curve in Figure 2 shows the free energy of adsorption of $Be(OH)_4^{2-}$ on the same surface. One energy minimum is found at $d_{CSH\text{-}Be} \approx 0.38$ nm (the surface complex **3a**). The sorption of $Be(OH)_4^{2-}$ is much stronger compared to $Be(OH)_3(OH_2)^-$ with an energy minimum of around −46 kJ/mol. Analysis of the coordination sphere at this distance reveals two surface calcium atoms involved in binding to the third one from the solution (RCN for the surface complex **3a** in Figure S3 in the Supporting Data). It can also be seen that the $Be(OH)_4^{2-}$ species does not form hydrogen bonds with (001) surface. The exchange of berylliums hydroxyls for oxygens of the silanol groups is possible, but it is not considered here a main sorption mechanism, because of several factors: a high concentration of surface calcium cations, unconstrained mobility of beryllium species on the surface, and the strong polarizability of the Be ion, which creates a stronger binding with its hydration sphere.

3.2. Sorption on the (004) Surface. The density profiles in the direction perpendicular to the (004) surface have been calculated and presented in Figure 3. The position of $d_{CSH} = 0$ nm for the (004) surface is defined as the average position of the topmost calcium atoms that belong to the structure of C-S-H (Ca_{CSH}).

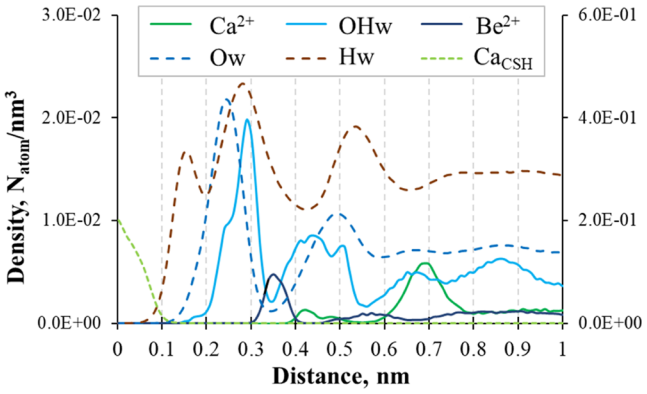

Figure 3. Atomic density profiles of solution species near the (004) C-S-H surface. The right-side axis shows densities plotted with dashed lines.

A peak of water hydrogens (Hw) is found at $d_{CSH\text{-}Hw} \approx 0.15$ nm followed by the peak of water oxygens (Ow) at $d_{CSH\text{-}Ow} \approx 0.21$ nm. Water forms a dense structured layer close to the surface through hydrogen bonding with surface oxygens. The highest oxygen peak of aqueous hydroxyls is found at $d_{CSH\text{-}OHw} \approx 0.29$ nm. These hydroxyls are bound to both the surface calcium layer and belong to the Be coordination sphere. The (004) surface is not as attractive for beryllium as the (001) surface, and most of the beryllium stayed in the solution during the 10 ns production run of the simulation (2 Be species sorbed on average). A small distinct peak is found at $d_{CSH\text{-}Be} \approx 0.3–0.4$ nm. This peak corresponds to the coordination of $Be(OH)_4^{2-}$ with surface calcium atoms. The formed surface complex could be identified from the two-dimensional density profiles in the solution layer at a distance of 0.1−0.5 nm from the surface (Figure S3 in the Supporting Information).

The free energy of adsorption of $Be(OH)_3(OH_2)^-$ and $Be(OH)_4^{2-}$ on the (004) C-S-H surface is shown in Figure 4. During the umbrella sampling simulations, the *xy* position on top of the surface was not constrained, and the species of Be were allowed to sample different orientation and binding possibilities on each distance from the surface. Overall, the sorption of both species is weaker and the energy barriers are lower than on the (001) surface.

Noticeably the $Be(OH)_3(OH_2)^-$ species form stable complexes by exchanging the water molecule for the bridging oxygen of the surface and coordinating two calcium through OH^- (the surface complex **1b**; $\Delta G_{min} = -16.30 \pm 1.67$ kJ/mol at $d_{CSH\text{-}Be} = 0.23$ nm). The energy needed for the exchange to happen is half that of the complexation on the (001) surface. Furthermore, the binding of beryllium to surface calcium only through the OH-bridge is not favorable for these species (the surface complex **2b**; $\Delta G_{min} = -6.27 \pm 0.04$ kJ/mol at $d_{CSH\text{-}Be} = 0.4$ nm).

The PMF curve for $Be(OH)_4^{2-}$ shows a much stronger complexation with the calcium layer exposed to the solution. The most favorable configurations are represented by the surface complexes **3b** and **4b** formed at $d_{CSH\text{-}Be} \approx 0.27$ and 0.38 nm, respectively. The surface complex **3b** corresponds to the binding with two surface calcium through two OH-bridges, while in the surface complex **4b** the two hydroxyls are coordinated with only one calcium. The second complex has the lowest energy ($\Delta G_{min} = -31.35 \pm 1.25$ kJ/mol), but the wideness of the minima shows that the two complexes are easily interchangeable. Together, they match the identified beryllium density peak at $d_{CSH\text{-}Be} \approx 0.3–0.4$ nm.

The (004) C-S-H surface may not provide the strongest sorption capabilities, but given the large surface area of C-S-H and the high stability of the (004) surface itself,[20] it will contribute significantly to the surface uptake of beryllium. Furthermore, in real C-S-H phases, this surface would contain defects in silicate chains that were not modeled in the current study, making the calcium layer more accessible for sorption and creating possibilities for additional Ca^{2+} cations and Be^{2+} hydroxide species to sorb.

3.3. Sorption on the (100) Surface. The edge surface of C-S-H has a less ordered molecular structure compared to other surfaces. It is not easy to define a zero position for the (100) surface because of its structural definition; thus, the structure of water layers could not be identified from the simple density profiles. However, the position of other ions still provides valuable information for describing sorption opportunities on this surface (Figure S5 in the Supporting Information). In the (100) surface model silicate layers are not aligned in the same plane; therefore, to avoid negative distance values, the zero position for the density profiles ($d_{CSH} = 0$ nm) is defined as an average position of the second from the solution density peak of Si atoms (Si_{CSH}). The missing bridging Si tetrahedra on this surface were also replaced with Ca^{2+}, with a total of 59 atoms of Ca on the surface after equilibration (60 atoms initially). Differently from the (001) surface, the Ca layer of C-S-H is also exposed to the solution at this interface.

Several peaks in the beryllium density profile could be seen which reveals multiple binding possibilities at the (100) surface. The time-averaged distributions of the atom in the layer parallel to the surface ($d < 0.6$ nm) are shown in Figure 5.

In the density profiles, beryllium is found close to the surface calcium atoms, similarly to the other surfaces. Both the $Be(OH)_3(OH_2)^-$ and $Be(OH)_4^{2-}$ species form stable complexes, and the complexation is mostly seen close to the

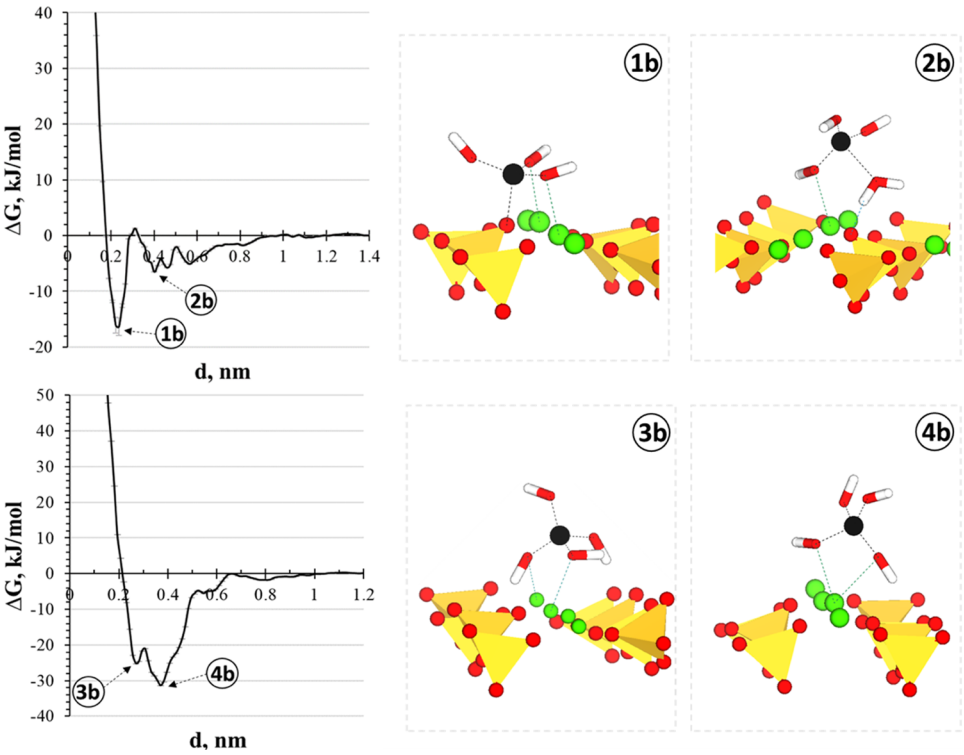

Figure 4. PMF curve for $Be(OH)_3(OH_2)^-$ (top) and $Be(OH)_4^{2-}$ (bottom) sorption on the (004) surface of C-S-H with snapshots of defined surface complexes (see Figure S4 in the Supporting Information for RCNs).

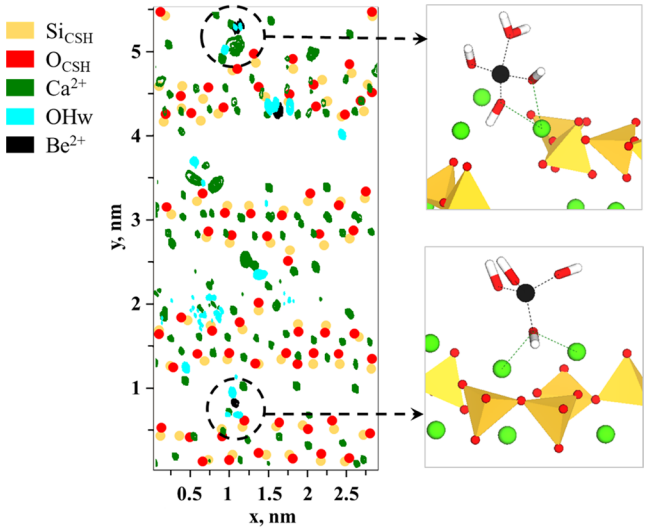

Figure 5. Atomic density contour maps of time-averaged surface distributions of selected atoms at d < 0.6 nm from the (100) C-S-H surface with the simulation snapshot of the surface complexes.

interlayer space. Of the 10 introduced beryllium species, 5 have sorbed on the (100) surface on average over the simulation time. The strength of this binding was further evaluated by calculating the PMF curves (Figure 6).

In the free energy profile for the $Be(OH)_3(OH_2)^-$ species, two main minima are seen at $d_{CSH\text{-}Be}$ 0.35 and 0.48 nm. The sorption is slightly weaker than on the (001) surface: the complexes were formed with a single surface calcium atom and the water molecule neither participated in binding nor was exchanged for silanol oxygen (RCN for the surface complexes **1c** and **2c** in Figure S6 in Supporting Information). The most stable complex of $Be(OH)_4^{2-}$ was formed by coordinating with three surface calcium atoms through OH-bridges (the surface complex **3c** at $d_{CSH\text{-}Be} \approx 0.23$ nm). The shallow minimum of around 0.6 nm with $\Delta G_{min} = -3.97 \pm 0.01$ kJ/mol corresponds to the formation of the outer-sphere complex.

The edge surface of C-S-H is much less ordered compared to the (001) and (004) surfaces. The distribution of charged groups is inhomogeneous, and the ions on this surface are potentially more mobile, which can explain the lower sorption energies found for both beryllium species.

In summary, sorption complexation with surface Ca in the C-S-H phases is one of the key mechanisms of the uptake of Be(II) by cementitious materials. The potential of mean force calculations allowed us to quantify and compare the strength of binding on different surfaces on the most common sorption sites. For all surfaces, the sorption energies were in the attractive range: $\Delta G_{min}(001) \approx -46$ kJ/mol, $\Delta G_{min}(004) \approx -31$ kJ/mol, and $\Delta G_{min}(100) \approx -17$ kJ/mol. On average, the $Be(OH)_4^{2-}$ species showed a higher retention affinity compared to the $Be(OH)_3(OH_2)^-$ species with the strongest surface complex formation with multiple Ca^{2+} cations at the (001) surface.

3.4. Sorption in the Interlayer. The study of sorption kinetics[17] revealed that the uptake of beryllium is stepwise: a fast surface complexation (within 4 days) followed by slow sorption, with equilibrium reached after 2 months. It was proposed that the slow uptake could be attributed to the incorporation of Be(II) into the C-S-H structure, and the most probable mechanism to consider is the uptake by the interlayer. Note that incorporation in the C-S-H interlayer has also been proposed for other strongly sorbing metal ions, e.g., Zn(II), Np(IV), Pu(IV).[4,51−54]

Molecular dynamics simulations were used to understand the behavior of $Be(OH)_3(OH_2)^-$ and $Be(OH)_4^{2-}$ in the C-S-

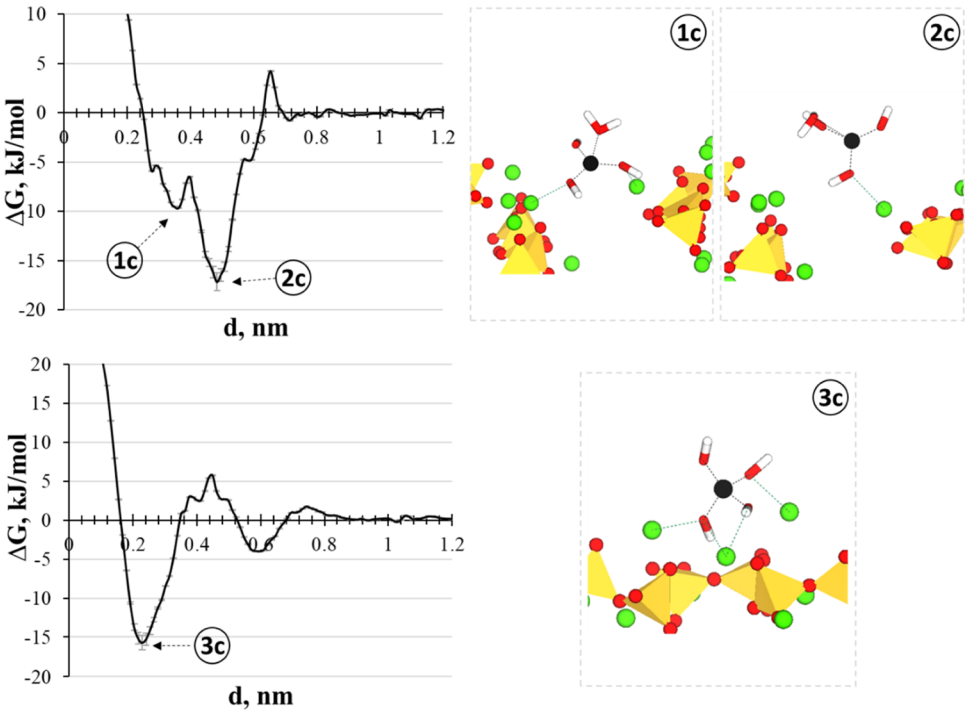

Figure 6. PMF curve for $Be(OH)_3(OH_2)^-$ (top) and $Be(OH)_4^{2-}$ (bottom) sorption on the (100) surface of C-S-H with snapshots of defined surface complexes (see Figure S6 in the Supporting Information).

H interlayer. First, the interlayer model was equilibrated without beryllium. Because of the high disorder in the structure, the interlayer distance varies greatly in the simulation cell, with an average of 1.17 nm. The introduction of 12 Be atoms did not change the interlayer distance.

The average atom densities for the four interlayers in the simulation cell were calculated, and the results are shown in Figure 7. The zero-distance position (d_{CSH} = 0 nm) is defined as the middle of the interlayer (the distance between two maximums of the Si_{CSH} atom density divided by two).

The density peaks for water and interlayer calcium are wide as a result of the disordered C-S-H structure. Similar to the results shown by Youssef et al.,[10] the hydrogen density peaks (Hw) of the interlayer water are positioned closer to the calcium silicate layer (Si_{CSH}) than the oxygen peaks (Ow) due

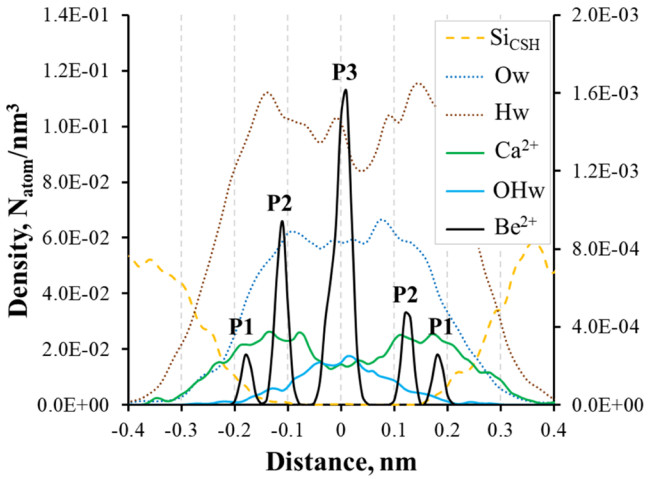

Figure 7. Atomic density profiles of solution species in the C-S-H interlayer. The right-side axis shows densities for Be^{2+}.

to the high number of the non-bridging oxygens in the structure. No well-defined layers of interlayer water can be seen in the calculated density profiles, and the formation of the water monolayer can be assumed, as was also described in Gaboreau et al.[21] There are two wide peaks of interlayer Ca, which correspond to calcium coordination with the calcium silicate layer in the positions of defects on the opposite interlayer surfaces. The positioning of interlayer calcium was found to be asymmetric: calcium cations are found mainly near the charged sites, where bridging silica tetrahedra were removed, confirming another suggestion made by Gaboreau et al.[21]

In contrast to calcium, the density profile of beryllium shows very defined sharp peaks. This behavior shows that beryllium is strongly immobilized in the interlayer space of C-S-H. The position of the Be peaks is symmetrical in the C-S-H interlayer. The detailed analysis of local time-averaged structures around individual Be atoms (Figure S7 in the Supporting Information) reveals three different binding positions (Figure 8):

(a) $Be(OH)_3^-$ is directly bound to one deprotonated silanol group and has 3−4 calcium atoms in the second coordination sphere (P1);
(b) $Be(OH)_3(OH_2)^-$ is coordinated through hydroxyl bridges with 3−4 interlayer calcium atoms and is found further from the surface (P2);
(c) $Be(OH)_4^{2-}$ is in the midplane of the interlayer space together with 4−5 calcium atoms in the second coordination sphere (P3).

The confined space of the interlayer allows the coordinated water molecule to exchange for the deprotonated silanol group, which was not observed for surface sorption. This could be compared with the results of Kremleva et al.,[55] where quantum chemical calculations were used to analyze uranyl(VI) sorption in the C-S-H interlayer with models based on 1.4 nm tobermorite. They showed that the sorption sites in the

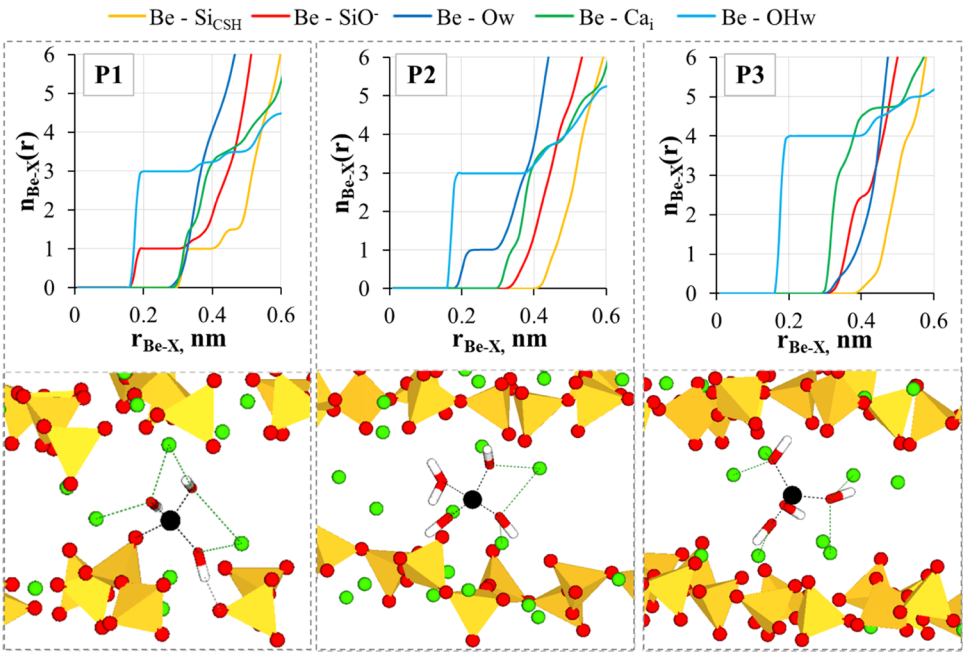

Figure 8. Running coordination numbers for Be pairs with the selected atoms types in the C-S-H interlayer and the corresponding simulation snapshots.

interlayer with the strongest compensating charge (i.e., with deprotonated silanol groups) are the most favorable for cation binding. Note, however, that in the case of beryllium, coordination with multiple oxygens from the silicate layer was not possible. This difference in behavior can be explained by the difference in the modeling approach: in this study beryllium was introduced in the interlayer as hydrolyzed species rather than as the Be^{2+} cation, whereas U(VI) was introduced as UO_2^{2+} in Kremleva et al.[55]

In the work of Lange et al.[56] ab initio simulations were performed to describe Ra^{2+} uptake in the C-S-H interlayer with model structures based on the 1.1 nm tobermorite with various interlayer calcium content. Their calculations showed that interlayer cation exchange is a likely Ra^{2+} uptake mechanism in C-S-H with low Ca/Si ratios. However, Be^{2+} has a much smaller ionic radius than Ca^{2+} or Ra^{2+}, and C-S-H with a high Ca/Si ratio is considered. No exchange of beryllium and calcium was observed in the simulation results, which also agrees with the measured effective cation exchange capacity of C-S-H with a high Ca/Si ratio.[57] Two factors could be synergetic: (i) interlayer calcium is strongly bound to the defect sites of the silica chains; (ii) beryllium has a strong hydration shell, that makes exchange energetically unfavorable. It can also be assumed that the main mechanism of incorporation is the interlayer uptake during C-S-H recrystallization.[4] Incorporation through the interlayer diffusion should be very slow and expectedly does not contribute significantly to overall uptake of beryllium.

4. CONCLUSIONS

The sorption mechanisms of beryllium on the (001), (004), and (100) surfaces of C-S-H with a high Ca/Si ratio (1.1:1.5) have been systematically studied using classical molecular dynamics simulations and the potential of mean force calculations. Aqueous speciation of Be(II) in a highly alkaline environment has been explicitly considered, and interface interactions of the two main hydrolysis species ($Be(OH)_3(OH_2)^-$ and $Be(OH)_4^{2-}$) were discussed in detail. Statistical analysis of the classical MD results allowed identification of the most common sorption sites and surface complexes of Be(II) species on each C-S-H surface considering its structural and energetic features.

Potential of mean force calculations were used then to evaluate the strength of binding with surface calcium and probability of ion exchange on the C-S-H interface. For all the surfaces studied the binding energies were in the attractive range between −46 and −12 kJ/mol. Sorption on the (001) surface of C-S-H was found to be the most favorable. The formation of Ca-hydroxyl bridges between surface calcium ions and beryllium was proven to be the main mechanism of surface binding for all the investigated surfaces.

Additionally, beryllium uptake in the C-S-H interlayer was analyzed, and it was found that beryllium does not substitute interlayer calcium at the defect sites of the silicate layer, but rather forms stable complexes through hydroxyl bridges. Beryllium showed very limited mobility in the interlayer, and we propose that the main process for the incorporation of Be(II) in the interlayer involves the recrystallization of the C-S-H phases. Further studies will be helpful to describe interlayer binding of beryllium species with an energetical perspective (e.g., DFT, ab initio MD calculations). The results of molecular dynamics simulations are consistent with reported experimental observations,[16−18] and support that both surface complex formation and incorporation into the C-S-H interlayer are relevant processes that result in strong beryllium uptake. The proposed approach will be extended to study the sorption behavior of other strongly hydrolyzing metal ions of relevance in the context of the nuclear waste disposal, e.g., Pu(IV), Am(III), or Tc(IV), on C-S-H phases with various Ca/Si ratios.

AUTHOR INFORMATION

Corresponding Author

Iuliia Androniuk − *Institute for Nuclear Waste Disposal (INE), Karlsruhe Institute of Technology (KIT), Eggenstein-Leopoldshafen 76344, Germany;* orcid.org/0000-0003-3189-4193; Email: iuliia.androniuk@kit.edu

Authors

Nese Çevirim-Papaioannou − *Institute for Nuclear Waste Disposal (INE), Karlsruhe Institute of Technology (KIT), Eggenstein-Leopoldshafen 76344, Germany*

Marcus Altmaier − *Institute for Nuclear Waste Disposal (INE), Karlsruhe Institute of Technology (KIT), Eggenstein-Leopoldshafen 76344, Germany*

Xavier Gaona − *Institute for Nuclear Waste Disposal (INE), Karlsruhe Institute of Technology (KIT), Eggenstein-Leopoldshafen 76344, Germany*

Notes

The authors declare no competing financial interest.

ACKNOWLEDGMENTS

The authors acknowledge support by the state of Baden-Württemberg through bwHPC and the German Research Foundation (DFG) through grant no INST 40/575-1 FUGG (JUSTUS 2 cluster).

REFERENCES

(1) Chandler, D.; Primm, R. T.; Maldonado, G. I.*Reactivity Accountability Attributed to Beryllium Reflector Poisons in the High Flux Isotope Reactor*, ORNL Report, TM-2009/188, Oak Ridge, USA, 2009.

(2) Longhurst, G. R.; Tsuchiya, K.; Dorn, C. H.; Folkman, S. L.; Fronk, T. H.; Ishihara, M.; Kawamura, H.; Tranter, T. N.; Rohe, R.; Uchida, M.; Vidal, E. Managing Beryllium in Nuclear Facility Applications. *Nucl. Technol.* **2011**, *176*, 430−441.

(3) Evans, N. D. M. Binding Mechanisms of Radionuclides to Cement. *Cem. Concr. Res.* **2008**, *38*, 543−553.

(4) Tits, J.; Wieland, E.*Actinide Sorption by Cementitious Materials*, PSI Technical Report, 18-02, Paul Schwerer Institute, Villigen, Switzerland, 2018.

(5) Garbev, K.; Bornefeld, M.; Beuchle, G.; Stemmermann, P. Cell Dimensions and Composition of Nanocrystalline Calcium Silicate Hydrate Solid Solutions. Part 2: X-Ray and Thermogravimetry Study. *J. Am. Ceram. Soc.* **2008**, *91*, 3015−3023.

(6) Pellenq, R. J. M.; Kushima, A.; Shahsavari, R.; Van Vliet, K. J.; Buehler, M. J.; Yip, S.; Ulm, F. J. A Realistic Molecular Model of Cement Hydrates. *Proc. Natl. Acad. Sci. U.S.A.* **2009**, *106*, 16102−16107.

(7) Hou, D.; Zhu, Y.; Lu, Y.; Li, Z. Mechanical Properties of Calcium Silicate Hydrate (C−S−H) at Nano-Scale: a Molecular Dynamics Study. *Mater. Chem. Phys.* **2014**, *146*, 503−511.

(8) Abdolhosseini Qomi, M.; Krakowiak, K.; Bauchy, M.; Stewart, K. L.; Shahsavari, R.; Jagannathan, D.; Brommer, D. B.; Baronnet, A.; Buehler, M. J.; Yip, S.; et al. Combinatorial Molecular Optimization of Cement Hydrates. *Nat. Commun.* **2014**, *5*, No. 4960.

(9) Androniuk, I.; Kalinichev, A. G. Molecular Dynamics Simulation of the Interaction of Uranium (VI) with the C-S-H Phase of Cement in the Presence of Gluconate. *Appl. Geochem.* **2020**, *113*, No. 104496.

(10) Youssef, M.; Pellenq, R. J. M.; Wildiz, B. Glassy Nature of Water in an Ultraconfining Disordered Material: The Case of Calcium-Silicate-Hydrate. *J. Am. Chem. Soc.* **2011**, *133*, 2499−2510.

(11) Arayro, J.; Dufresne, A.; Zhou, T.; Ioannidou, K.; Ulm, J.-F.; Pellenq, R.; Béland, L. K. Thermodynamics, Kinetics, and Mechanics of Cesium Sorption in Cement Paste: a Multiscale Assessment. *Phys. Rev. Mater.* **2018**, *2*, No. 053608.

(12) Qomi, M. J. A.; Brochard, L.; Honorio, T.; Maruyama, I.; Vandamme, M. Advances in Atomistic Modeling and Understanding of Drying Shrinkage in Cementitious Materials. *Cem. Concr. Res.* **2021**, *148*, No. 106536.

(13) Marx, D.; Sprik, M.; Parrinello, M. Ab Initio Molecular Dynamics of Ion Solvation. The Case of Be^{2+} in Water. *Chem. Phys. Lett.* **1997**, *273*, 360−366.

(14) Alderighi, L.; Gans, P.; Midollini, S.; Vacca, A. Aqueous Solution Chemistry of Beryllium. *Adv. Inorg. Chem.* **2000**, *50*, 109−172.

(15) Perera, L. C.; Raymond, O.; Henderson, W.; Brothers, P. J.; Plieger, P. G. Advances in Beryllium Coordination Chemistry. *Coord. Chem. Rev.* **2017**, *352*, 264−290.

(16) Çevirim-Papaioannou, N.; Gaona, X.; Böttle, M.; Bethune Yalcintas, E.; Schild, D.; Adam, C.; Sittel, T.; Altmaier, M. Thermodynamic Description of Be(II) Solubility and Hydrolysis in Acidic to Hyperalkaline NaCl and KCl Solutions. *Appl. Geochem.* **2020**, *117*, No. 104601.

(17) Çevirim-Papaioannou, N.; Androniuk, I.; Han, S.; Ait Mouheb, N.; Gaboreau, S.; Um, W.; Gaona, X.; Altmaier, M. Sorption of Beryllium in Cementitious Systems Relevant for Nuclear Waste Disposal: Quantitative Description and Mechanistic Understanding. *Chemosphere* **2021**, *282*, No. 131094.

(18) Çevirim-Papaioannou, N.; Han, S.; Androniuk, I.; Um, W.; Altmaier, M.; Gaona, X. Uptake of Be(II) by Cement in Degradation Stage I: Wet-Chemistry and Molecular Dynamics Studies. *Minerals* **2021**, *11*, No. 1149.

(19) Biagioni, C.; Merlino, S.; Bonaccorsi, E. The Tobermorite Supergroup: a New Nomenclature. *Mineral. Mag.* **2015**, *79*, 485−495.

(20) Mutisya, S. M.; Miranda, C. R. The Surface Stability and Morphology of Tobermorite 11 Å From First Principles. *Appl. Surf. Sci.* **2018**, *444*, 287−292.

(21) Gaboreau, S.; Grangeon, S.; Claret, F.; Ihiawakrim, D.; Ersen, O.; Montouillout, V.; Maubec, N.; Roosz, C.; Henocq, P.; Carteret, C. Hydration Properties and Interlayer Organization in Synthetic C-S-H. *Langmuir* **2020**, *36*, 9449−9464.

(22) Svenum, I.-H.; Ringdalen, I. G.; Bleken, F. L.; Friis, J.; Hoeche, D.; Swang, O. Structure, Hydration, and Chloride Ingress in C-S-H: Insight from DFT Calculations. *Cem. Concr. Res.* **2020**, *129*, No. 105965.

(23) Jamil, T.; Javadi, A.; Heinz, H. Mechanism of Molecular Interaction of Acrylate- Polyethylene Glycol Acrylate Copolymers with Calcium Silicate Hydrate Surfaces. *Green Chem.* **2020**, *22*, 1577−1593.

(24) Cong, X. D.; Kirkpatrick, R. J. Si-29 MAS NMR Study of The Structure of Calcium Silicate Hydrate. *Adv. Cem. Based Mater.* **1996**, *3*, 144−156.

(25) Roosz, C.; Vieillard, P.; Blanc, P.; Gaboreau, S.; Gailhanou, H.; Braithwaite, D.; Montouillout, V.; Denoyel, R.; Henocq, P.; Madé, B. Thermodynamic Properties of C-S-H, C-A-S-H and M-S-H Phases: Results from Direct Measurements and Predictive Modelling. *Appl. Geochem.* **2018**, *92*, 140−156.

(26) Churakov, S. V.; Labbez, C.; Pegado, L.; Sulpizi, M. Intrinsic Acidity of Surface Sites in Calcium Silicate Hydrates and Its Implication to Their Electrokinetic Properties. *J. Phys. Chem. C* **2014**, *118*, 11752−11762.
(27) Cygan, R. T.; Liang, J.-J.; Kalinichev, A. G. Molecular Models of Hydroxide, Oxyhydroxide, and Clay Phases and the Development of a General Force Field. *J. Phys. Chem. B* **2004**, *108*, 1255−1266.
(28) Cygan, R. T.; Greathouse, J. A.; Kalinichev, A. G. Advances in Clayff Molecular Simulation of Layered and Nanoporous Materials and Their Aqueous Interfaces. *J. Phys. Chem. C* **2021**, *125*, 17573−17589.
(29) Kalinichev, A. G.; Wang, J. W.; Kirkpatrick, R. J. Molecular Dynamics Modeling of the Structure, Dynamics and Energetics of Mineral-Water Interfaces: Application to Cement Materials. *Cem. Concr. Res.* **2007**, *37*, 337−347.
(30) Mishra, R. K.; Mohamed, A. K.; Geissbuhler, D.; Manzano, H.; Jamil, T.; Shahsavari, R.; Kalinichev, A. G.; Galmarini, S.; Tao, L.; Heinz, H.; et al. Cemff: a Force Field Database for Cementitious Materials Including Validations, Applications and Opportunities. *Cem. Concr. Res.* **2017**, *102*, 68−89.
(31) Zhakiyeva, Z.; Cuello, G. J.; Fischer, H. E.; Bowron, D. T.; Dejoie, C.; Magnin, V.; Campillo, S.; Bureau, S.; Poulain, A.; Besselink, R.; et al. Structure of Water Adsorbed on Nanocrystalline Calcium Silicate Hydrate Determined from Neutron Scattering and Molecular Dynamics Simulations. *J. Phys. Chem. C* **2022**, *126*, 12820−12835.
(32) Berendsen, H. J. C.; Grigera, J. R.; Straatsma, T. P. The Missing Term in Effective Pair potentials. *J. Phys. Chem. A* **1987**, *91*, 6269−6271.
(33) Li, P. F.; Merz, K. M., Jr. Taking into Account the Ion-Induced Dipole Interaction in the Nonbonded Model of Ions. *J. Chem. Theory Comput.* **2014**, *10*, 289−297.
(34) Li, Z.; Song, L. F.; Li, P. F.; Merz, K. M., Jr. Systematic Parametrization of Divalent Metal Ions for the OPC3, OPC, TIP3P-fb, and TIP4P-fb Water Models. *J. Chem. Theory Comput.* **2020**, *16*, 4429−4442.
(35) Kirkpatrick, R. J.; Kalinichev, A. G.; Hou, X.; Struble, L. Experimental and Molecular Dynamics Modeling Studies of Interlayer Swelling: Water Incorporation in Kanemite and ASR Gel. *Mater. Struct.* **2005**, *38*, 449−458.
(36) Kirkpatrick, R. J.; Kalinichev, A. G.; Wang, J. Molecular Dynamics Modelling of Hydrated Mineral Interlayers and Surfaces: Structure and Dynamics. *Mineral. Mag.* **2005**, *69*, 289−308.
(37) Allen, M. P.; Tildesley, D. J.*Computer Simulation of Liquids*, 2nd ed.; Oxford University Press: New York, 2017.
(38) Plimpton, S. Fast Parallel Algorithms for Short-Range Molecular Dynamics. *J. Comput. Phys.* **1995**, *117*, 1−19.
(39) Braun, E.; Gilmer, J.; Mayes, H. B.; Mobley, D. L.; Monroe, J. I.; Prasad, S.; Zuckerman, D. M. Best Practices for Foundations in Molecular Simulations [article v1.1]. *Living J. Comput. Mol. Sci.* **2019**, *1*, No. 5957.
(40) Humphrey, W.; Dalke, A.; Schulten, K. VMD: Visual Molecular Dynamics. *J. Mol. Graphics* **1996**, *14*, 33−38.
(41) Bonaccorsi, E.; Merlino, S.; Kampf, A. R. The Crystal Structure of Tobermorite 14 A (Plombierite), a C−S−H Phase. *J. Am. Ceram. Soc.* **2005**, *88*, 505−512.
(42) Kovačević, G.; Nicoleau, L.; Nonat, A.; Veryazov, V. Revised Atomistic Models of the Crystal Structure of C−S−H with High C/S Ratio. *Z. Phys. Chem.* **2016**, *230*, 1411−1424.
(43) Gartner, E.; Maruyama, I.; Chen, J. A New Model for the C-S-H Phase Formed During the Hydration of Portland Cements. *Cem. Concr. Res.* **2017**, *97*, 95−106.
(44) Grangeon, S.; Claret, F.; Linard, Y.; Chiaberge, C. X-Ray Diffraction: a Powerful Tool to Probe and Understand the Structure of Nanocrystalline Calcium Silicate Hydrates. *Acta Crystallogr., Sect. B: Struct. Sci., Cryst. Eng. Mater.* **2013**, *69*, 465−473.
(45) Kästner, J. Umbrella Sampling. *Wiley Interdiscip. Rev.: Comput. Mol. Sci.* **2011**, *1*, 932−942.
(46) Fiorin, G.; Klein, M. L.; Hénin, J. Using Collective Variables to Drive Molecular Dynamics Simulations. *Mol. Phys.* **2013**, *111*, 3345−3362.
(47) Grossfield, A.An Implementation of WHAM: The Weighted Histogram Analysis Method, Version 2.0.9, 2014.
(48) Grossfield, A.; Patrone, P. N.; Roe, D. R.; Schulz, A. J.; Siderius, D. W.; Zuckerman, D. M. Best Practices for Quantification of Uncertainty and Sampling Quality in Molecular Simulations [Article V1.0]. *Living. J. Comput. Mol. Sci.* **2018**, *1*, No. 5067.
(49) Viallis-Terrisse, H.; Nonat, A.; Petit, J.-C. Zeta-Potential Study of Calcium Silicate Hydrates Interacting with Alkaline Cations. *J. Colloid Interface Sci.* **2001**, *244*, 58−65.
(50) Labbez, C.; Pochard, I.; Jönsson, B.; Nonat, A. C-S-H/Solution Interface: Experimental and Monte Carlo Studies. *Cem. Concr. Res.* **2011**, *41*, 161−168.
(51) Ziegler, F.; Giere, R.; Johnson, C. A. Sorption Mechanisms of Zinc to Calcium Silicate Hydrate: Sorption and Microscopic Investigations. *Environ. Sci. Technol.* **2001**, *35*, 4556−4561.
(52) Ziegler, F.; Scheidegger, A. M.; Johnson, C. A.; Dahn, R.; Wieland, E. Sorption Mechanisms of Zinc to Calcium Silicate Hydrate: X-Ray Absorption Fine Structure (XAFS) Investigation. *Environ. Sci. Technol.* **2001**, *35*, 1550−1555.
(53) Gaona, X.; Dahn, R.; Tits, J.; Scheinost, A. C.; Wieland, E. Uptake of Np(IV) by C-S-H Phases and Cement Paste: an EXAFS Study. *Environ. Sci. Technol.* **2011**, *45*, 8765−8771.
(54) Häußler, V.; Amayri, S.; Beck, A.; Platte, T.; Stern, T. A.; Vitova, T.; Reich, T. Uptake of Actinides by Calcium Silicate Hydrate (C-S-H) Phases. *Appl. Geochem.* **2018**, *98*, 426−434.
(55) Kremleva, A.; Krüger, S.; Rösch, N. Uranyl(VI) Sorption in Calcium Silicate Hydrate Phases. A Quantum Chemical Study of Tobermorite Models. *Appl. Geochem.* **2019**, *113*, No. 104463.
(56) Lange, S.; Kowalski, P. M.; Pšenička, M.; Klinkenberg, M.; Rohmen, S.; Bosbach, D.; Deissmann, G. Uptake of 226Ra in Cementitious Systems: A Complementary Solution Chemistry and Atomistic Simulation Study. *Appl. Geochem.* **2018**, *96*, 204−216.
(57) Bernard, E.; Yan, Y.; Lothenbach, B. Effective Cation Exchange Capacity of Calcium Silicate Hydrates (C-S-H). *Cem. Concr. Res.* **2021**, *143*, No. 106393.